Supporting Information

Differential Glycosylation does not modulate the Conformational Heterogeneity of Humanised IgGk NIST Monoclonal Antibody

Fanny C. Liu,*[a] Jusung Lee,[a] Thais Pedrete,[a] Erin M. Panczyk,[b] Stuart Pengelley[c] and Christian Bleiholder*[a,d]

[a.]Department of Chemistry and Biochemistry, Florida State University, 102 Varsity Way, Tallahassee, Florida, 32306, USA.

[b.]Bruker Daltonics, 40 Manning Road, Billerica, MA 01821, USA.

[c.]Bruker Daltonics GmbH&Co, Fahrenheitstrasse 4, Bremen, 28359, Germany.

[d.]Institute of Molecular Biophysics, Florida State University, 91 Chieftan Way, Tallahassee, Florida, 32306, USA.

*corresponding authors. E-mails: cbleiholder@fsu.edu; fliu@fsu.edu

Figure S1. Mass spectrum recorded for NISTmAb with (A) gentle instrument settings and (B) collisional activation in Tandem-TIMS depicts charge states 23+ to 28+. The inset shows the glycoform pattern of charge state 25+ when recorded with collisional activation settings.

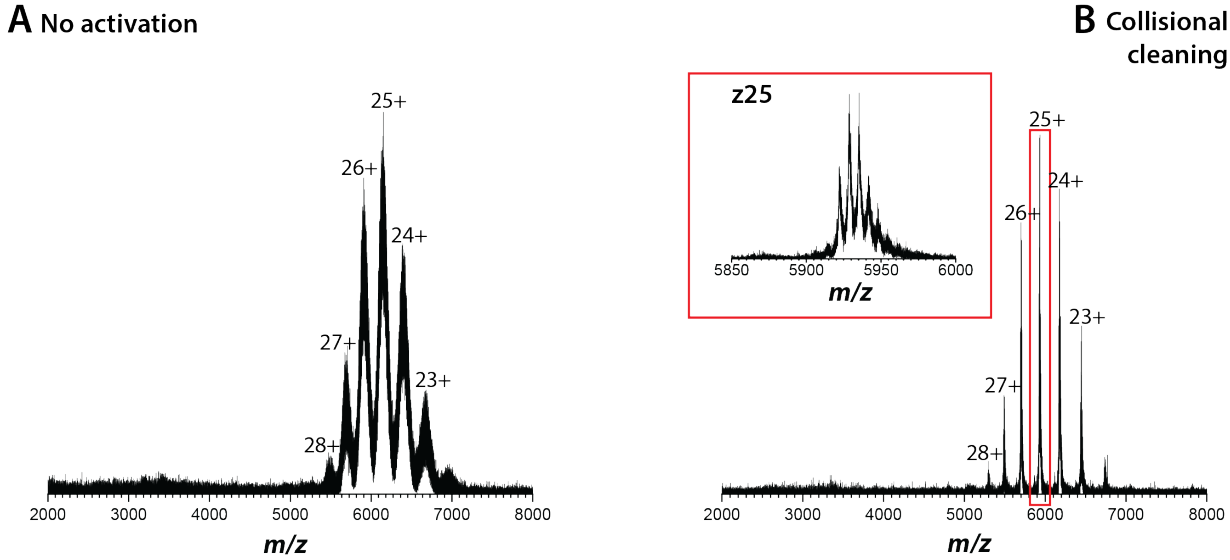
A No activation
25+
26+
24+
27+
23+
28+
2000
3000
4000
5000
6000
7000
8000
m/z
B Collisional cleaning
z25
5850
5900
5950
6000
m/z
25+
24+
26+
23+
27+
28+
2000
3000
4000
5000
6000
7000
8000
m/z

Figure S2. Comparison of cross-sections for various NISTmAb charge states measured in Tandem-TIMS and an RF confining drift tube IMS[1].

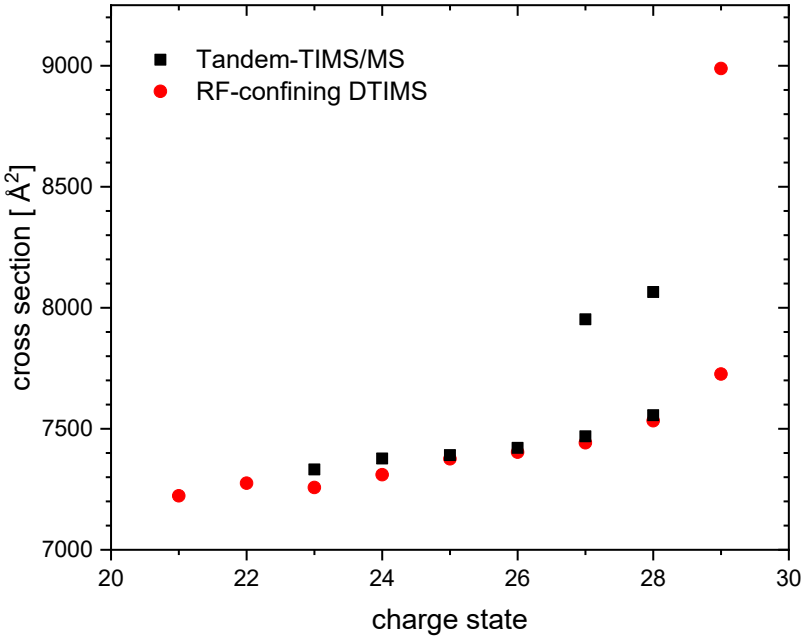

Table S1. Cross sections of NISTmAb with various charge states recorded in Tandem-TIMS and an RF-confining Drift tube IMS.[1] Nitrogen was used as buffer gas.

Charge state	Tandem-TIMS [Å²]	RF-DTIMS[1] [Å²]
21	-	7223
22	-	7275
23	7332	7257
24	7377	7310
25	7391	7376
26	7421	7403
27	7469	7442
	7952	
28	7556	7533
	8065	
29	-	7726
		8988

Figure S3. Deconvoluted mass spectrum of NISTmAb recorded in Tandem-TIMS/MS under activating instrumental settings showing well-resolved glycoforms.

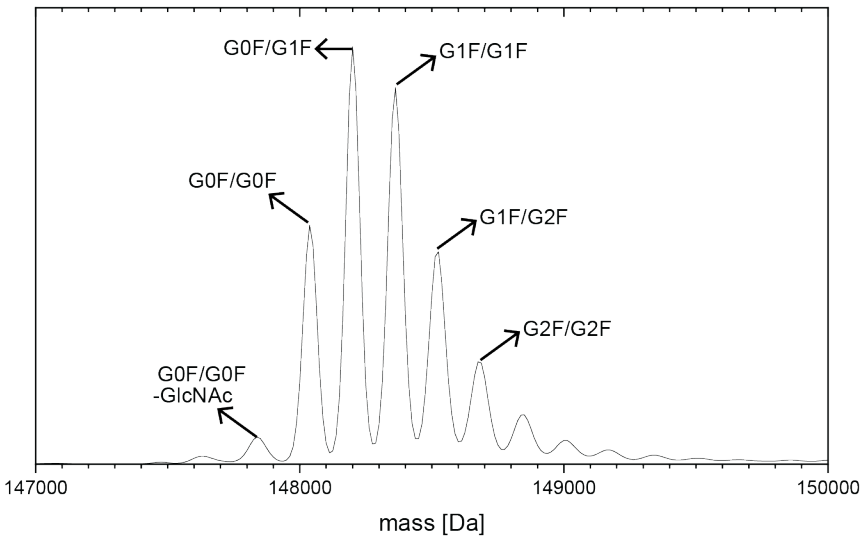

Table S2. Deconvolved masses of NISTmAb glycoforms recorded in Tandem-TIMS/MS and their respective errors in ppm.

Glycoform	Theoretical MW (Da)	Recorded MW (Da)	Error (ppm)
G0F/G0F-GlcNAc	147,834.0	147,837.9	26.4
G0F/G0F	148,037.2	148,037.5	2.0
G0F/G1F	148,199.3	148,200.0	4.7
G1F/G1F	148,361.4	148,362.5	7.4
G1F/G2F	148,523.6	148,524.9	8.8
G2F/G2F	148,685.7	148,687.5	12.1

G0 = GlcNAc2Man3GlcNAc2
G0F = GlcNAc2Man3GlcNAc2Fuc
G1F = GalGlcNAc2Man3GlcNAc2Fuc
G2F = Gal2GlcNAc2Man3GlcNAc2Fuc

Figure S4. The ensemble average collisional-induced unfolding of NISTmAb charge state 26+ in Tandem-TIMS.

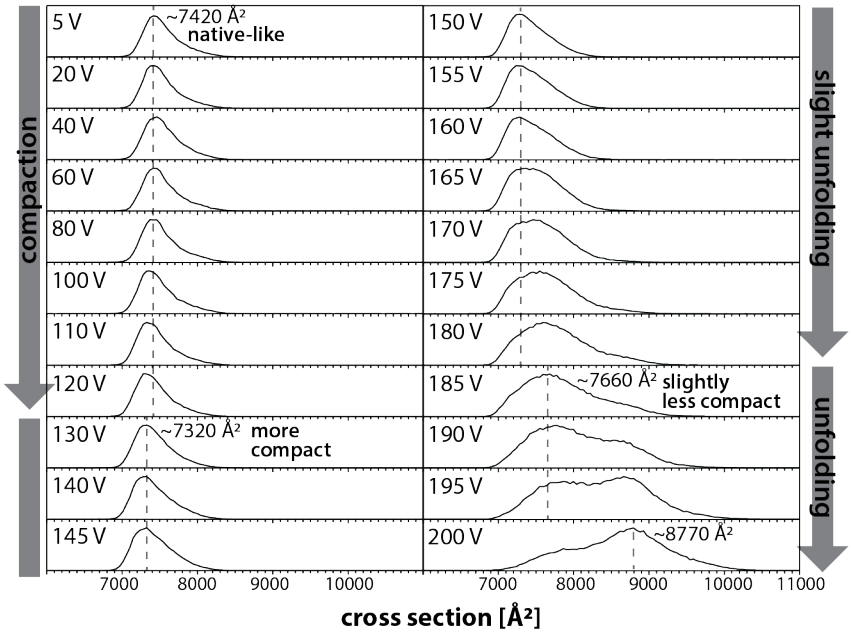

Figure S5. Ion mobility spectra (left) and the fraction of native contacts (right) computed by the SRA for charge states 23+ (black traces), 26+ (red traces), and 27+ (blue traces). Note that due to the significant computational demand, the prediction of ion mobility spectra produced upon vibrational activation was only carried out for charge state 26+ (red traces).

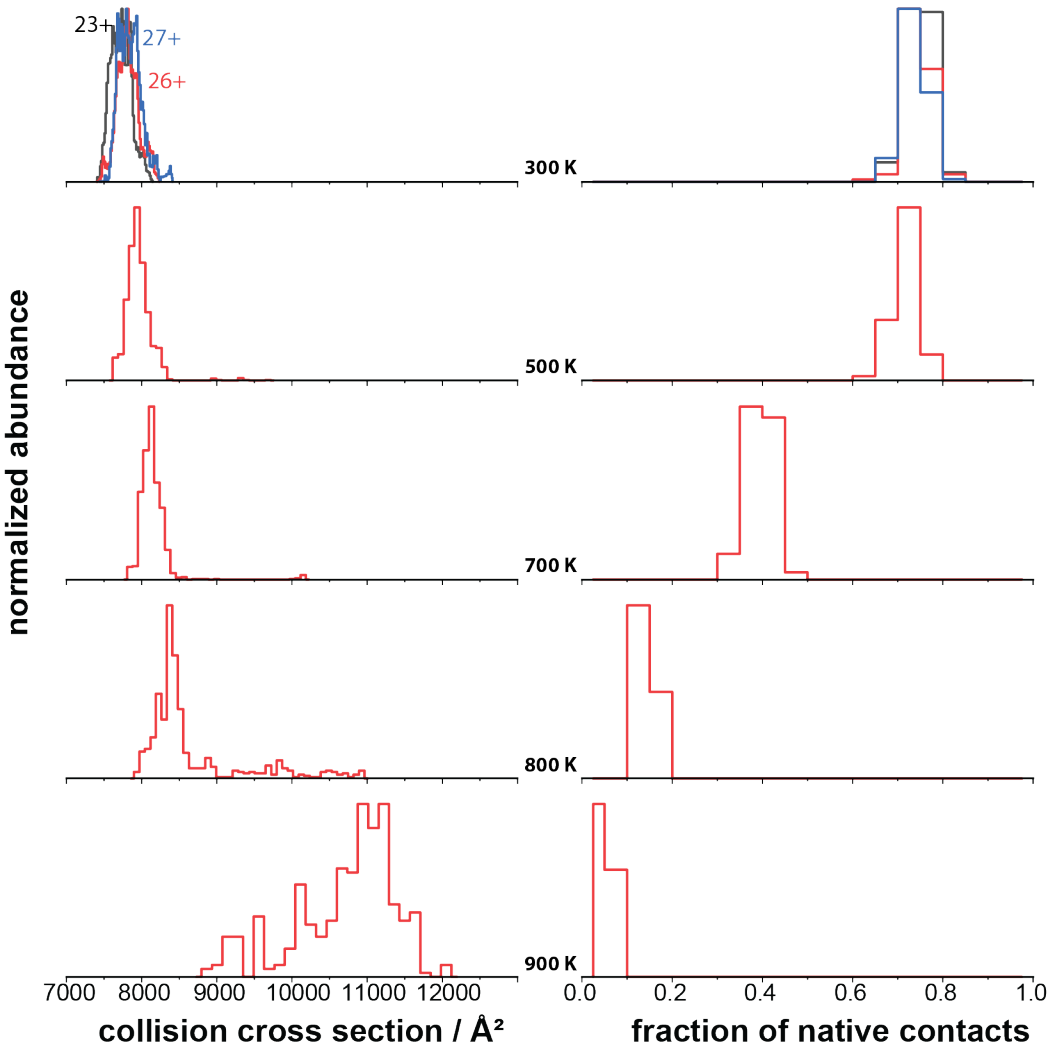

Figure S6. Detailed three-dimensional structures of the unfolded NISTmAb in solvent-free environment can be obtained by the Structure Relaxation Approximation (SRA) method.

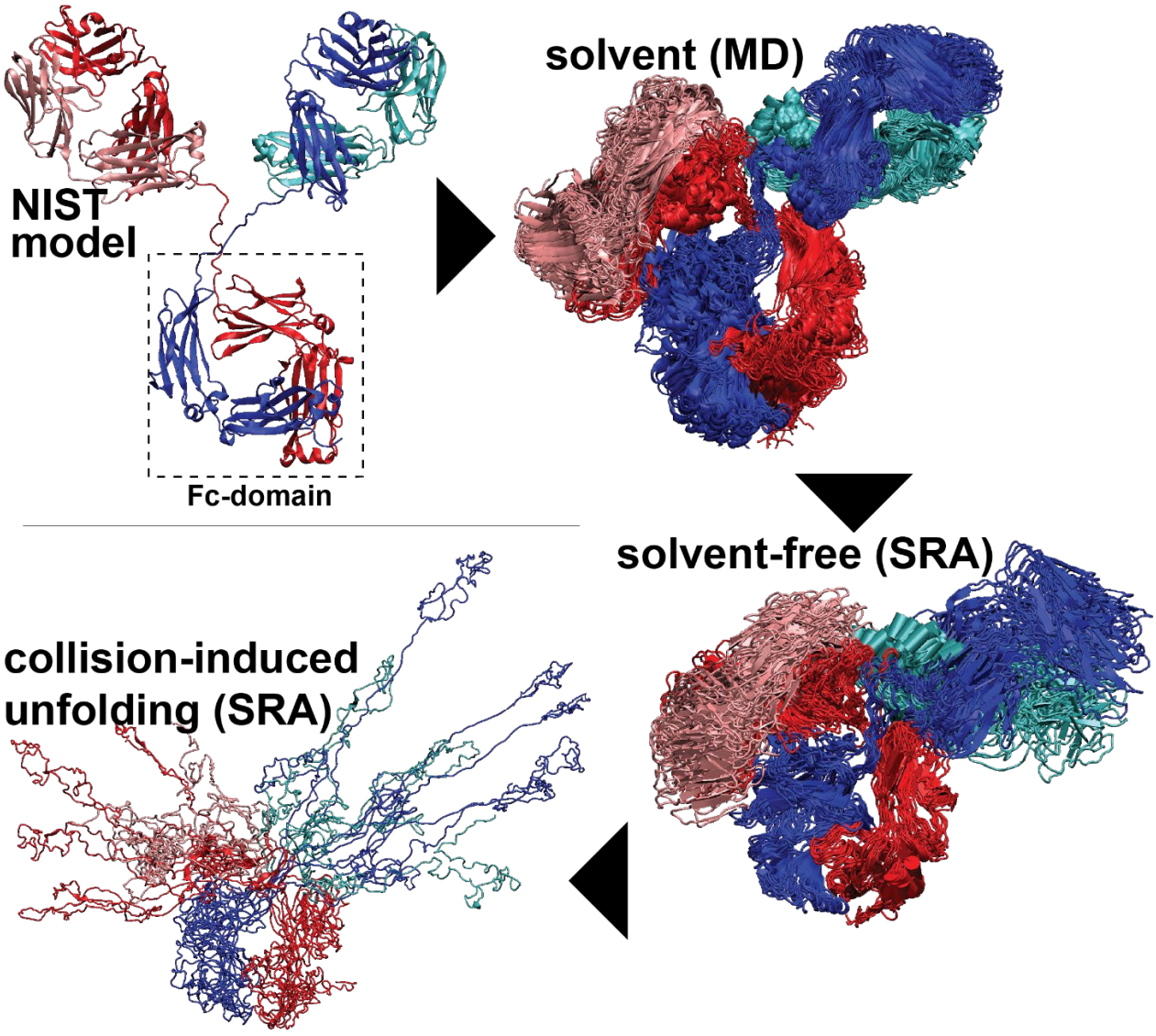

(top, left) The NIST model of NISTmAb built from the Fab and Fc crystal structures (PDB codes 5K8A and 5VGP) with hinge from PDB 1IGT with heavy chains (red, blue) and light chains (cyan, pink) color-coded. (top, right) Solution-phase dynamics as assessed per explicit-solvent molecular dynamics simulations. Figure shows superimposed snapshots sampled during the MD simulations. (bottom, right) Our SRA method proposes that the structural heterogeneity is largely retained in the solvent-free environment for native-like charge state 26+ without collisional activation. (bottom, left) Our SRA method proposes that collisional activation increases the collision cross-section of NISTmAb because the components of the Fab domain unfold while the Fc-domain continues to hold the heavy chains together.

Figure S7. The SRA-calculated fraction of native contacts is correlated with the calculated increase in collision cross section due to vibrational activation for charge state 26+ as shown in Figure S6.

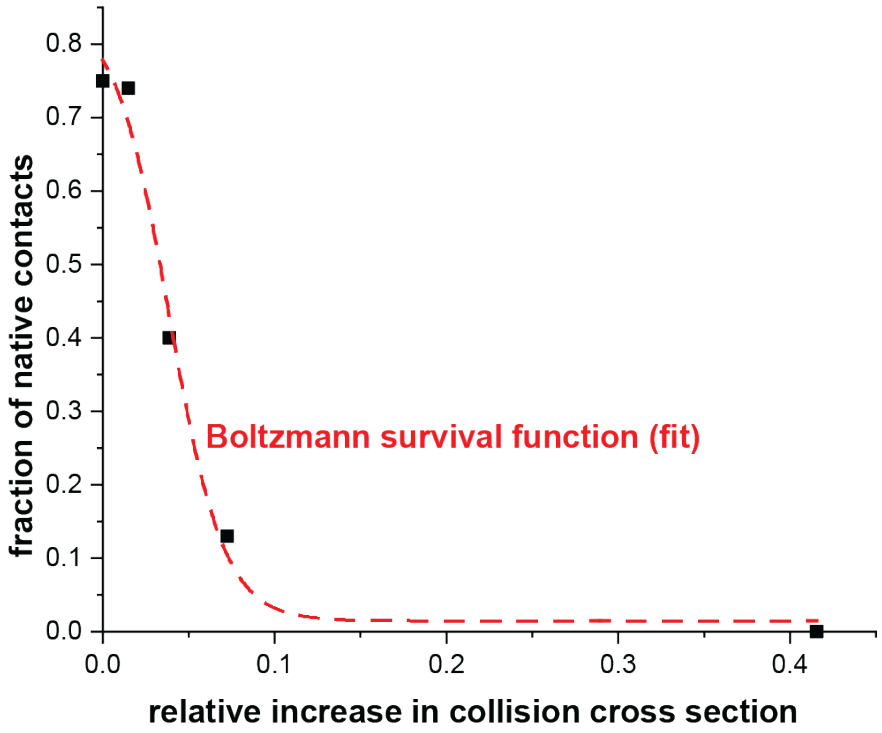

Table S3. The number of solvent adducts retained in the subpopulations of NISTmAb charge state 26+ at various activation voltages. The average m–z of subpopulation 1 at an activation voltage of 5 V is essentially identical to that obtained at 80 V for subpopulation 2 (m–z ~5880).

Activation voltage	Subpopulation 1		Subpopulation 2	
	Average m–z	Approximate number of water adducts	Average m–z	Approximate number of water adducts
5	5880	255	5893	272
20	5882	257	5890	269
40	5882	257	5890	269
60	5883	259	5885	262
80	5873	243	5881	255
100	5841	198	5858	222
110	5821	169	5841	198
120	5800	139	5820	168
130	5783	114	5800	138
140	5767	91	5782	113
145	5759.1	80	5774	101
150	5752.5	70	5766	89
155	5745.8	60	5758	78
160	5740.9	53	5750	67
165	5733.2	42	5744	58
170	5728.7	36	5739	51
175	5724.1	29	5733	42
180	5719.7	23	5728	35
185	5718.8	21	5727	33
190	5715.3	16	5722	25
195	5712.8	13	5718	20
200	5710.9	10	5716	17

Figure S8. Investigating the structural heterogeneity of NISTmAb by non-ensemble measurements in Tandem-TIMS. (A) The ion mobility peak of NISTmAb charge state 25+ (black trace) is superimposed with four subpopulations obtained by mobility-selection (dark blue, red, light blue, and light brown traces), each corresponding to a distinct collision cross-section. The subpopulations are kinetically stable for at least ~50-100 ms in the absence of bulk solvent, which indicates that these NISTmAb species do not interconverting at least on that time-scale. (B) Subpopulations of NISTmAb charge state 25+ exhibit identical glycoforms with almost identical ratios. (C) The average m-~~z~~ of subpopulation 1 at an activation voltage of 20 V is identical to that obtained at 80 V for subpopulation 2 (m-~~z~~~6125). (D) Despite having the same mass and, thus, the same number of attached solvent adducts, the subpopulations maintain the differences in their collision cross-sections of ~ 7 %.

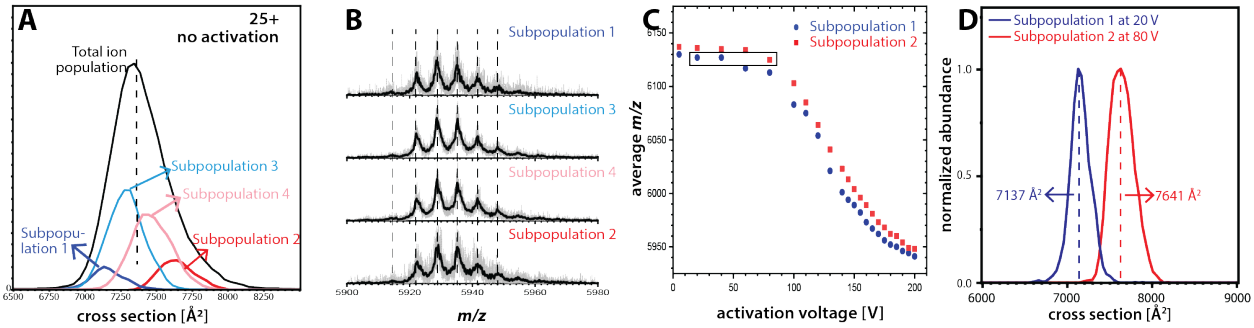

Figure S9. Mobility-resolved CIU spectra of NISTmAb charge state 26+ in Tandem-TIMS.

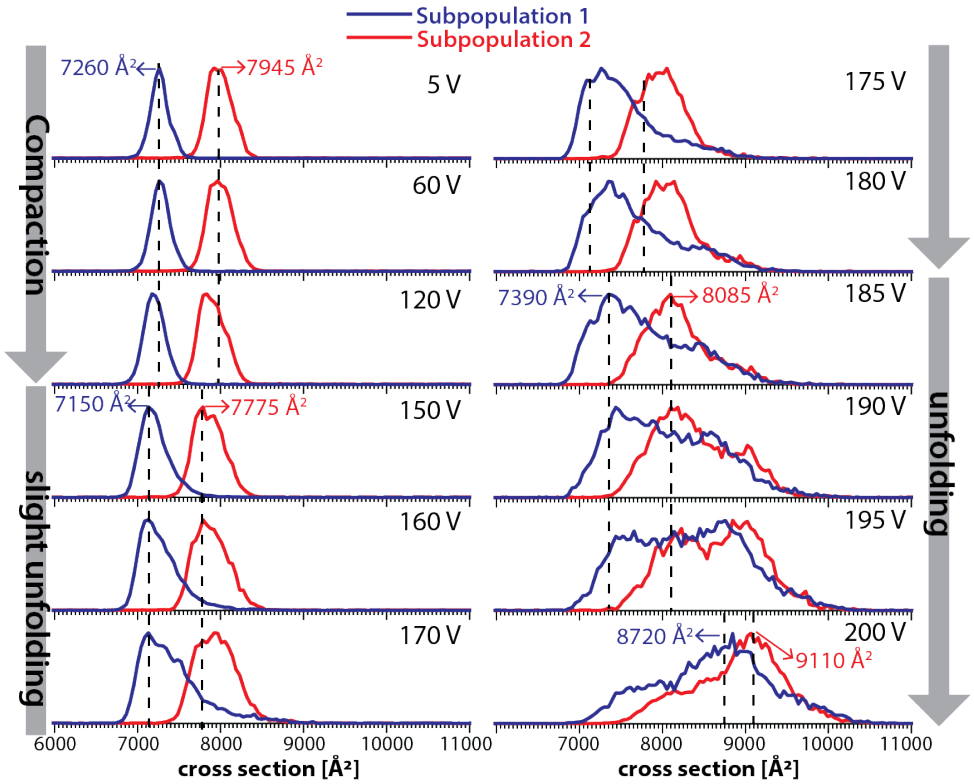

Figure S10. Mobility-resolved CIU spectra of NISTmAb charge state 25+ in Tandem-TIMS.

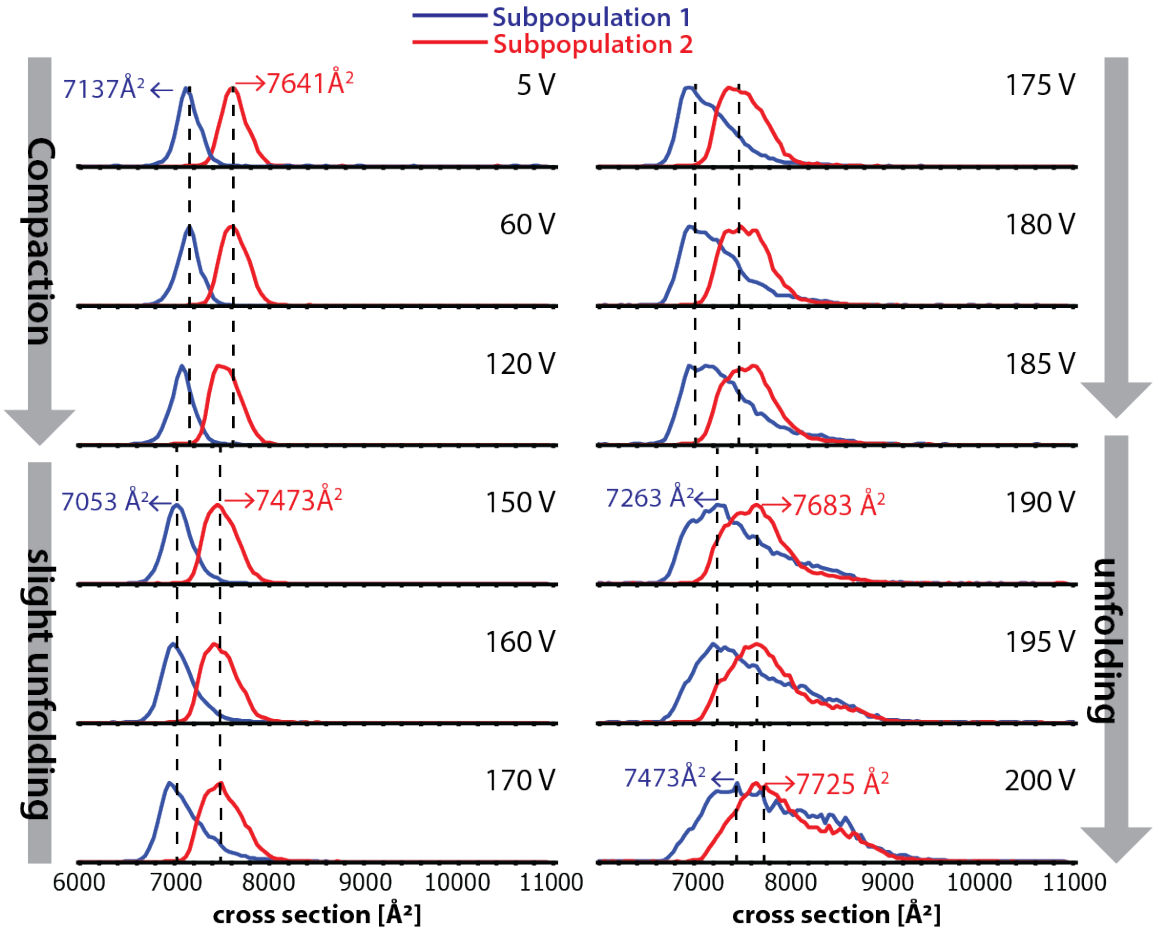

Molecular dynamics simulations

Explicit solvent molecular dynamics simulations. The proposed NISTmAb structure[2] was subjected to explicit solvent molecular dynamics simulations to generate a conformational ensemble as input for the computation of ion moblity spectra using the structure relaxation approximation (SRA, below). Using GROMACS, we carried out explicit solvent molecular dynamics simulations using the OPLS/AA force field[4,5] and periodic boundary conditions as described previously.[3] Briefly, the NISTmAb structure was placed in a 122 Å x 159 Å x 188 Å box filled with 16019 TIP3P water models, 220 Na^+ and 234 Cl^- ions for charge neutralisation. After equilibration, eight trajectories were propagated for an aggregate simulation time of 3.2 μs with structures saved every 1 ns for subsequent analysis. The first 200 ns of each trajectory were discarded from analysis. From the remaining snapshots, 500 structures were randomly selected as input for the SRA, as described below.

Structure Relaxation Approximation (SRA). The SRA employs sequential molecular dynamics simulations that are carried out for a duration of t_{step} (given as input; with initial velocities generated from Boltzmann distributions) starting from 300 K and increasing in steps of T_{step} until the maximal temperature T_{max} (given as input) is reached. The system is then propagated at temperature T_{max} for a duration of t_{max} and cooled down in steps of T_{step} until the final temperature of 300K is reached. The final simulation was then performed for t_{final} at 300 K with structures saved every 10 ps for further analysis. For the calculation of NISTmAb ion mobility spectra, we used the previously reported settings (T_{max}=600 K, T_{step}=100 K, t_{final}=2 ns). We used the GROMACS 4.5.7 simulation package to carry out all gas phase simulations in conjunction with the OPLS-AA[4,5] force field following previous publications.[3,6,7] Neither periodicity nor cut-offs were employed for these simulations and the relative permittivity was set to 1.0. Energy conservation was achieved using a 1 fs integration step and constraining bonds to hydrogen with the LINCS algorithm.[8] Detailed settings for the MD simulations are found in the Supporting Information to reference [7].

Figure S11. Structural heterogeneity of NISTmAb in the presence and absence of solvent.

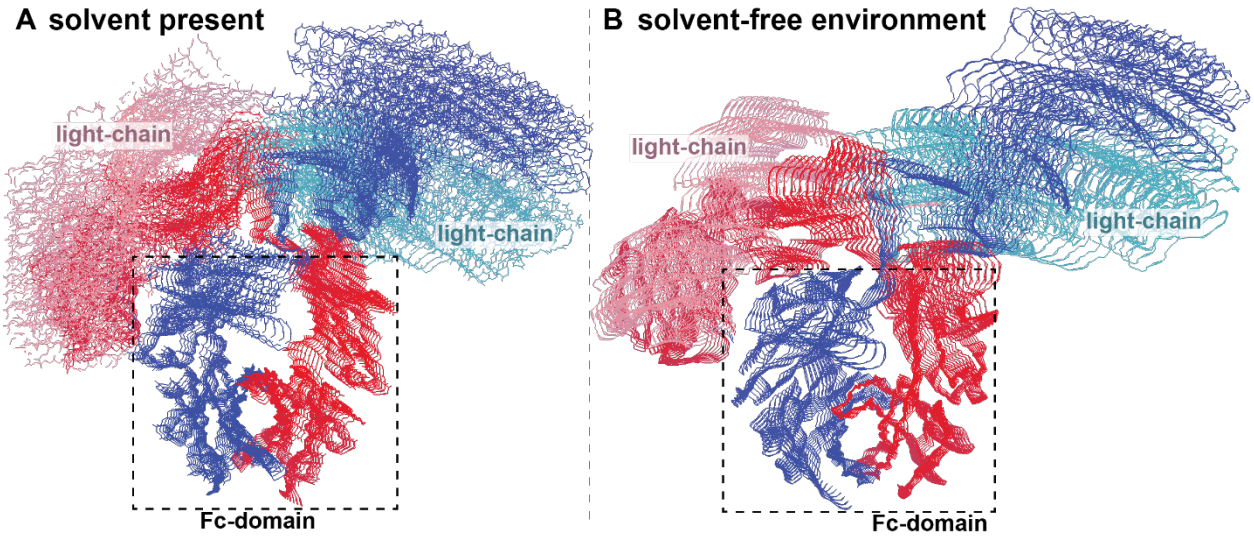

To compare the structural heterogeneity of the NISTmAb ensembles computed for the solvent-present and solvent-free environments, we analysed the eigenvectors obtained from principal

component analysis of the covariance matrix. Figure S11A plots the NISTmAb motions associated with the dominant eigenvector obtained from the explicit-solvent MD simulations, mainly associated with the angle between the Fc and Fab domains. Figure S11B plots the equivalent eigenvector observed for the solvent-free NISTmAb structural ensemble computed by the SRA for charge state 26+. Our data thus indicate that some aspects of the solution-phase structural heterogeneity and dynamics of NISTmAb are preserved upon transfer into the solvent-free environment of our Tandem-TIMS instrument.

References

(1) Campuzano, I. D. G.; Larriba, C.; Bagal, D.; Schnier, P. D. Ion Mobility and Mass Spectrometry Measurements of the Humanized IgGk NIST Monoclonal Antibody. In ACS.Symposium.Series; Schiel, J. E., Davis, D. L., Borisov, O. V., Eds.; American Chemical Society: Washington, DC, 2015; Vol. 1202, pp 75–112. https://doi.org/10.1021/bk-2015-1202.ch004.

(2) Bergonzo, C.; Gallagher, D. T. Atomic Model Structure of the NIST Monoclonal Antibody (NISTmAb) Reference Material. J¡. Res¡. Natl¡. Inst¡. Stand¡. Technol¡ 2021, 78❷, 126012. https://doi.org/10.6028/jres.126.012.

(3) Cropley, T. C.; Liu, F. C.; Pedrete, T.; Hossain, M. A.; Agar, J. N.; Bleiholder, C. Structure Relaxation Approximation (SRA) for Elucidation of Protein Structures from Ion Mobility Measurements (II). Protein Complexes. J¡. Phys¡. Chem¡. B 2023, 78❸ (25), 5553–5565. https://doi.org/10.1021/acs.jpcb.3c01024.

(4) Jorgensen, W. L.; Tirado-Rives, J. The OPLS Potential Functions for Proteins. Energy Minimizations for Crystals of Cyclic Peptides and Crambin. J¡.Am¡.Chem¡.Soc¡ 1988, 776, 1657–1666.

(5) Kaminski, G. A.; Friesner, R. A.; Tirado-Rives, J.; Jorgensen, W. L. Evaluation and Reparametrization of the OPLS-AA Force Field for Proteins via Comparison with Accurate Quantum Chemical Calculations on Peptides. J¡. Phys¡. Chem¡. B 2001, 76❶ (28), 6474–6487. https://doi.org/10.1021/jp003919d.

(6) Hall, Z.; Politis, A.; Bush, M. F.; Smith, L. J.; Robinson, C. V. Charge-State Dependent Compaction and Dissociation of Protein Complexes: Insights from Ion Mobility and Molecular Dynamics. J¡. Am¡.Chem¡.Soc¡ 2012, 790 (7), 3429–3438. https://doi.org/10.1021/ja2096859.

(7) Bleiholder, C.; Liu, F. C. Structure Relaxation Approximation (SRA) for Elucidation of Protein Structures from Ion Mobility Measurements. J¡. Phys¡. Chem¡. B 2019, 789 (13), 2756–2769. https://doi.org/10.1021/acs.jpcb.8b11818.

(8) Hess, B.; Bekker, H.; Berendsen, H. J. C.; Fraaije, J. G. E. M. LINCS: A Linear Constraint Solver for Molecular Simulations. J¡. Comput¡. Chem¡ 1997, 7❹ (12), 1463–1472. https://doi.org/10.1002/(SICI)1096-987X(199709)18:12<1463::AID-JCC4>3.0.CO;2-H.